Appendix C

Simulation of Radial Expansion of an Electron Beam Injected into a Background Plasma

J. Koga and C. S. Lin
Department of Space Sciences
Southwest Research Institute
San Antonio, Texas 78284

Abstract

A two-dimensional electrostatic particle code has been used to study the beam radial expansion of a nonrelativistic electron beam injected from an isolated equipotential conductor into a background plasma. The simulations indicate that the beam radius is generally proportional to the beam electron gyroradius when the conductor is charged to a large potential. The simulations also suggest that the charge buildup at the beam stagnation point causes the beam radial expansion. From a survey of the simulation results, it is found that the ratio of the beam radius to the beam electron gyroradius increases with the square root of beam density and decreases inversely with beam injection velocity. This dependence is explained in terms of the ratio of the beam electron Debye length to the ambient electron Debye length. These results are most applicable to the SEPAC electron beam injection experiments from Spacelab 1, where high charging potential was observed.

INTRODUCTION

Over the past 10 years, nonrelativistic electron beams have been injected into a background plasma and neutral gas to study beam propagation, instabilities, spacecraft charging, and other space plasma problems in the ionosphere [1–5]. Some experiments specifically studied the radial expansion characteristics of the beam [2–3], indicating that the beam expansion characteristics depend in a complex way on beam propagation angle and spacecraft charging. Many simulation studies have examined the general relationship between spacecraft charging and the electron beam injection in the ionosphere [6–12]. However, few have focused on understanding the radial expansion phenomenon. The purpose of this paper is to report our simulation study on the beam radial expansion.

In the Vehicle Charging and Potential (VCAP) experiment on the Space Shuttle Orbiter mission, the STS-3 camera imaged a narrow collimation of an electron beam fired transverse to the magnetic field for 0.3m before the light emission of the electron beam abruptly decreased [2–3]. The reason for the sudden decrease in light emissions is unclear. However, it may suggest that appreciable beam radial expansion seemed to occur due to an increase in the negative charge density of the beam. After the point of beam spreading, the beam evolved into a hollow cylindrical shell structure which propagated parallel to the local magnetic field. The vehicle electric potential induced by these electron beam firings was normally a few volts to a few tens of volts with a beam energy of 1 keV [2].

Space Experiments with Particle Accelerators (SEPAC) during the Spacelab 1 mission indicated that the electron beam injection had charged the spacecraft to a potential as high as the beam energy, which was 5 keV [5]. Because the ambient plasma cannot neutralize the electron beam and the spacecraft, the net beam charge and the spacecraft charging are important in this case for determining beam propagation and expansion.

In laboratory experiments, Kellogg et al. [4] studied radial expansion of electron beams injected into a background plasma and neutral gas. When the electron gun was grounded, the envelope of the beam was twice the beam electron gyroradius ρ_e where $\rho_e = v_b/\Omega_{ce}$ for cross-field injection. For the aligned beam the radius of the envelope was $r_b \approx 0.25\rho_e$. However, when the electron gun was allowed to float and no background plasma was present, the electron

beam appeared to have a diameter approximately twice the beam electron gyroradius. In these cases the gun potential rose to the electron beam accelerator potential. Therefore, charging seems to play an important role in the beam radial expansion.

Several two-dimensional simulations show that high density electron beams can propagate in the plasma because the net beam charge has caused the beam to expand radially and reduced the beam density [9–12]. In particular, Winglee and Pritchett [11] have simulated cross-field and parallel electron beam injection, concentrating on moderate spacecraft charging. For cross-field injection the beam is found to form a hollow cylinder of radius approximately equal to the beam gyroradius and width of about $2\lambda_{Db}$ where $\lambda_{Db} = v_b/\omega_b$. The beam width is believed to be caused by repulsive forces associated with a net negative charge within the beam. For parallel injection slower beam electrons are overtaken, causing a net repulsive force repelling the beam electrons outward to a cylinder thickness comparable to the cross-field injection case. The maximum perpendicular velocity was found to be comparable to the parallel beam velocity.

Analytic calculations [13] for electron beams injected parallel to magnetic field lines have shown that space charge effects play an important role during the initial phase of beam expansion. Furthermore, the magnetic field determines the beam radius and beam density. However, the calculations did not take into account any possible beam instabilities.

In this paper we study radial expansion of electron beams injected parallel to the magnetic field. We have used a two-dimensional electrostatic particle code to simulate the electron beam injection from an isolated finite equipotential conductor into a plasma. In contrast to Winglee and Prichett [12], we concentrate on cases of high spacecraft charging, which are more applicable to SEPAC electron beam firings. It is shown that radial expansion is significant. We also surveyed the simulation results to determine the dependence of the beam expansion on the background magnetic field, beam density, and beam velocity.

SIMULATION MODEL

To study electron beam injection from a conductor, we modified a 2-D particle-in-cell code, DARWIN, which was originally developed at Los Alamos National Laboratory

[14]. Here we present the simulation results in the electrostatic limit. Realistic modeling of beam injection from a spacecraft required injecting an electron beam from a finite isolated conductor. The simulation geometry is shown in Figure 1.

Particles are injected from the spacecraft surface in the simulation box every time step. The number of injected electrons per time step per cell is $N_c(e/q_e)(n_b/n_c)v_b\Delta t$ where N_c is the number of ambient electrons per cell, Δt is the simulation time step, n_b/n_c is the ratio of the beam density to ambient density, and e/q_e is the ratio of the ambient electron charge to the beam electron charge. The beam electrons have fractional charge and mass, which allows an increase in the number injected per time step. This larger number for the same beam density reduces numerical noise. These particles are placed in the simulation box at positions $x = Rv_b\Delta t$ where x is the distance from the conductor surface, v_b is the injection velocity, and R is a random number between 0 and 1 for each injected particle. This method tends to fill in the fan between $x = 0$ and $x = v_b\Delta t$. The injected particles are randomly distributed across the beam in the y direction. All particles which strike the spacecraft surface are absorbed and their charge is accumulated.

Treating the spacecraft surface as a finite isolated equipotential conductor in an ambient plasma was accomplished by using the capacity matrix method [11,15]. The capacity matrix relates the charge on each grid point on the spacecraft to the corresponding potential.

$$q_i = \sum_j C_{ij}\Phi_j \tag{1}$$

where C_{ij} is the capacity matrix, Φ_j is the spacecraft potential, and the sum j is over every grid point on the spacecraft. The capacity matrix is found by placing a unit charge on one point of the spacecraft surface with all other points zero and then solving for the potential. The values of the potential at each point on the spacecraft represent one column in the inverse capacity matrix $A = C^{-1}$. Repeating the process for each node then generates the full inverse matrix. The capacity matrix is obtained from the inverse of this matrix. This process is carried out only once at the beginning of the program. During the program the code first solves Poisson's equation for the electric potential Φ_0 with charge evenly distributed on the spacecraft surface. Second, it uses the capacity matrix of the conductor to redistribute the

charge and maintain the spacecraft surface at an equipotential using the formulae:

$$\Delta q_i = \sum_j C_{ij}(\Phi_{eq} - \Phi_{0j}) \tag{2}$$

$$\Phi_{eq} = \sum_{ij} C_{ij} / \sum_{ij} C_{ij} \tag{3}$$

where Δq_i is the charge that is added to each grid point on the spacecraft. Using the redistributed charge density, the code again solves Possion's equation for the electric potential of the spacecraft.

We use a periodic boundary condition for the lower boundary at $y = 0$ and the upper boundary at $y = L_y$ where L_y is the simulation length in the y direction. The electrostatic potential at $x = 0$, $\phi(x = 0, y)$, is constant. We assume the potential is zero at the right boundary at $x = L_x$ where L_x is the simulation length in the x direction. The right boundary condition approximates the potential at infinity.

Ambient ions and electrons are initialized uniformly in the system with a uniform magnetic field in the x direction. Both the ambient ions and electrons have Maxwellian velocity distributions with the same temperature, $T_e = T_i$ where T_e and T_i are the electron and ion temperatures, respectively. At the right and left boundary, the code specularly reflects all particles.

SIMULATION RESULTS

The simulation uses a $512\Delta \times 128\Delta$ grid in the x and y directions, respectively. The spacecraft is represented by a rectangular box centered on $x = 102\Delta$ and $y = 64\Delta$ with size $4\Delta \times 32\Delta$ in the x and y directions, respectively. The grid size, Δ, equals the Debye length of the ambient electrons defined as $\lambda_d = a_c/\omega_{pe}$ where $a_c = (2T_e/m_e)^{1/2}$ is the thermal velocity of the ambient electrons and ω_{pe} is the ambient electron plasma frequency. We choose the ion to electron mass ratio to be 100, and $a_c = 0.001c$ where c is the speed of light, a unit of the simulation. We use a reference electron gyrofrequency Ω_{ce} of $0.25\omega_{pe}$, which is close to the ionospheric value of $0.3\omega_{pe}$. The simulations use a time step $\Delta t = 0.05\omega_{pe}^{-1}$ and 131,072 particles for the ambient plasma. For the reference case the electron beam has a width of 4Δ,

an injection velocity of $v_b = 10a_c$ along the x axis, zero initial thermal velocity, and a density ratio of $n_b/n_c = 10$.

Figures 2-4 show results of electron beam injection for the reference parameters. The phase space plot $x - v_x$ at $\omega_{pe}t = 30$ in Figure 2a indicates that the point at which beam electrons are stopped (stagnation point) is very close to the conductor surface. Due to the high beam density the spacecraft becomes positively charged, causing the beam electrons to be rapidly drawn back to the spacecraft surface. The average electrostatic potential of the spacecraft in this case is $\approx$ 94% of the beam energy. Some electrons at the front of the beam are accelerated to velocities higher than the original beam velocity. This is due to the bunching of beam electrons behind the beam head. Also some returning beam electrons overshoot the spacecraft and are drawn back on the wake side. The configuration space plot given in Figure 2b shows that the electron beam expands radially. Figure 3a shows a contour plot of the beam density where the contour line delineates the beam edge. From this plot the beam radius is approximately $r_b = 40\Delta$. The beam electron gyroradius $\rho_e = v_b/\Omega_{ce}$ is also 40Δ where v_b is the initial beam velocity. It is apparent from earlier configuration space plots that the maximum beam expansion occurs near the stagnation point, which is very close to the spacecraft surface. The highest beam density is at the stagnation point of the beam (Figure 3b). This is in agreement with analytical results for one dimensional electron beam injection into a vacuum [16]. Physically, the high density at the stagnation point is understood in an approximate sense by the conservation of flux $n_b v_b$. At the stagnation point, where the average beam velocity is smallest, the density should be highest assuming substantial expansion of the beam has not occurred.

Figure 4a and 4b show that the maximum transverse electric field E_y and the maximum longitudinal electric field E_x occur where the beam density is highest. The transverse velocities to which the beam electrons are accelerated depends on the time spent in the stagnation region, where the transverse electric fields are largest. This can be estimated from the width of the transverse electric field region, approximately 8Δ, and the initial beam velocity. From these values it is apparent that the beam particles can be accelerated to 75% of the initial beam velocity. In general beam electrons travel through the stagnation region with velocities

lower than the initial beam velocity. So they spend more time in the stagnation region and are accelerated to higher velocities. After the stagnation region the transverse electric field E_y is smaller (Figure 4a) and the average beam velocity is higher (Figure 2a). Therefore, the beam electrons receive their largest tranverse kick very close to the spacecraft and experience smaller transverse impulses from that point on.

Variation with Magnetic Field Strength

Figure 5 shows beam density plots at $\omega_{pe}t = 30$ where the contour lines indicate the beam envelope. The magnetic field Ω_{ce}/ω_{pe} is 0.25, 0.5, and 1.0 down the page with all other parameters fixed. Note that the maximum beam radius decreases with increasing magnetic field. The ratio of the maximum beam radius to the electron gyroradius r_b/ρ_e is approximately 1 for each of these cases. This indicates that independent of the magnetic field the beam electrons receive the same transverse kick and expand to ρ_e in the range of ionospheric magnetic field values. In Figure 5c, where $\Omega_{ce}/\omega_{pe} = 1.0$, no beam electrons are in the wake region of the spacecraft. The maximum width beam electrons achieve, $2\rho_e$, is smaller than the spacecraft width. So all returning beam electrons strike the spacecraft surface.

Variation with Beam Density

Figure 6 shows simulation results at $\omega_{pe}t = 30$ varying the beam to ambient plasma density ratio n_b/n_c from 1 to 20 for the cases of $\Omega_{ce}/\omega_{pe} = 0.25$ (solid line) and 0.5 (dotted line). The ratio r_b/ρ_e is between 0.725 for $n_b/n_c = 1$ and 1.3 for $n_b/n_c = 20$. The maximum beam radius gradually increases with beam density. This indicates that the transverse kick that the beam electrons receive gradually increases with beam density. The relative magnitude of the transverse kick can be obtained from the average velocity of the beam electrons through the stagnation region. The average velocity gives a rough idea of the time that the beam electrons are accelerated by the transverse electric fields E_y in the stagnation region. Figure 7 shows the average velocity of beam electrons at the stagnation point versus beam density for $\Omega_{ce}/\omega_{pe} = 0.25$ (solid line) and 0.5 (dotted line) at $\omega_{pe}t = 30$. The velocity is averaged across the beam and the stagnation point is taken to be the point where the longitudinal

electric field E_x is a maximum. The average velocity decreases with increasing beam density for both values of magnetic field. This indicates that beam electrons spend more time in the stagnation region for higher density beams and are, therefore, accelerated to higher transverse velocities. The ratio of the electron beam Debye length λ_{Db} to the ambient electron Debye length λ_d, which is

$$\frac{\lambda_{Db}}{\lambda_d} = (\frac{v_b}{a_c})(\frac{n_c}{n_b})^{1/2}, \tag{4}$$

gives an understanding of this velocity trend. The electron beam Debye length is an indication of the charge separation distance between the spacecraft and the beam stagnation point. The ambient electron Debye length indicates the distance above which ambient electrons neutralize excess charge. As this ratio decreases the beam electrons feel the Coulombic potential of the spacecraft more since ambient electrons have a harder time shielding the effects of the retarding potential drop. Therefore, the beam electrons travel with lower velocities. This ratio decreases with increasing beam density n_b as $n_b^{-1/2}$ following the trend of the average velocity in Figure 7.

Variation with Beam Velocity

Figure 8 shows the beam radius normalized to the electron gyroradius r_b/ρ_e as a function of initial injection velocity v_b at $\omega_{pe}t = 30$. The injection velocity v_b/a_c where a_c is the ambient electron thermal velocity is varied between 2.5 and 20.0. All other parameters are the same as in the reference case. The radial expansion is largest for small velocity injection and smallest for high velocity injection. The relative magnitude of the transverse kick can again be inferred from the average velocity of the beam electrons through the stagnation region. Figure 9 shows the average velocity of beam electrons at the stagnation point versus initial beam injection velocity at $\omega_{pe}t = 30$. The average velocity increases with the initial beam injection velocity. Beam electrons spend more time in the stagnation region for lower injection velocities and are, therefore, accelerated to higher relative transverse velocities. This velocity trend can also be interpreted from the ratio of the beam electron Debye length to the ambient electron Debye length. This ratio increases linearly with the initial beam injection velocity. As the

beam injection velocity increases, the ambient electrons are more able to shield excess charge buildup over the beam electron Debye length. Therefore, the beam electrons travel with higher velocities through the stagnation region, which is in agreement with Figure 9.

DISCUSSION AND CONCLUSION

We have examined the radial expansion properties of a nonrelativistic electron beam injected along magnetic field lines into a background plasma. We have concentrated on high beam current cases where spacecraft charging is significant. In our reference case with $n_b/n_c = 10$ and $v_b/a_c = 10$, the beam expanded to twice the beam electron gyroradius ρ_b. The beam electrons receive a large transverse kick from beam electrons which have built up at the stagnation point. This kick, which occurs very close to the injection point, determines the beam envelope from that point on. We have found that the transverse energization of the beam electrons is independent of the strength of the magnetic field for values between $\Omega_{ce}/\omega_{pe} = 0.25$ and 1. The beam envelope is twice the beam electron gyroradius ρ_e. We have also found that the beam envelope increases with beam density. The average velocity of beam electrons through the stagnation region decreases with increasing beam density. The average velocity indicates the time beam electrons spend in the stagnation region and, therefore, how long beam electrons are accelerated by the transverse electric fields. The final transverse velocity of the beam electrons and, thus, the beam envelope increases with beam density. Variation of the initial beam injection velocity indicates that the beam envelope decreases with increasing beam injection velocity. The average velocity of beam electrons through the stagnation region increases with beam injection velocity. Therefore, beam electrons with high injection velocity are accelerated to lower relative transverse velocities than beam electrons with low injection velocities. The ratio of λ_{Db}/λ_d, which is an indication of how well beam electrons are shielded from the charged spacecraft surface by the ambient electrons, can be used to explain the dependence of beam radius on beam density and beam injection velocity. This dependence is evident from Figure 7 where the average beam velocity at the stagnation point drops off approximately as $n_b^{-1/2}$ and from Figure 9 where the average velocity increases almost linearly with beam injection velocity v_b.

The spacecraft potential energy in each of these runs varied between 60% and 100% of the beam energy except for the cases of low beam density. These results are most applicable to the SEPAC electron beam injection experiments where the Shuttle was charged to the beam energy. In future work we will address the problem of beam radial expansion when collisional ionizations of neutrals by the beam electrons is taken into account.

ACKNOWLEDGMENTS

The authors would like to thank R. M. Winglee for collaboration on simulation techniques. The work was supported by NASA contract NAGW–1231. The particle simulations were performed on the CRAY-YMP at NASA Ames Research Center.

REFERENCES

[1] B. Grandal, ed., " Artificial Particle Beams in Space Plasma Studies", Plenum, New York, 1982.

[2] P. M. Banks, W. J. Raitt, A. B. White, R. I. Bush, and P. R. Williamson, "Results from the vehicle charging and potential experiment on STS-3", *J. Spacecr. Rockets*, vol. 24, p. 138, 1987.

[3] P. M. Banks and W. J. Raitt, "Observations of electron beam structure in space experiments", *J. Geophys. Res.*, vol. 93, p. 5811, 1988.

[4] P. J. Kellogg, H. R. Anderson, W. Bernstein, T. J. Hallinan, H. R. Holzworth, R. J. Jost, H. Leinbach, and E. P. Szuszuczewicz, "Laboratory simulation of injection particle beams in the ionosphere", *Artificial Particle Beams in Space Plasma Studies*, edited by Bjorn Grandel, 1982, pp. 289-329.

[5] S. Sasaki, N. Kawashima, K. Kuriki, M. Yanagisawa, and T. Obayashi, "Vehicle charging observed in SEPAC Spacelab-1 experiment", *J. Spacecr. Rockets*, vol. 23, no. 2, p. 129, 1986.

[6] Y. Omura, and H. Matsumoto, "Computer simulations of beam injection experiments for SEPAC/Spacelab 1 mission", *Radio Sci.*, vol. 19, no. 2, p. 496, 1984.

[7] P. L. Pritchett, and R. M. Winglee, "The plasma environment during particle beam injection into space plasmas, 1, electron beams", *J. Geophys. Res.*, vol. 92, no. A7, p. 7673, 1987.

[8] H. Okuda, and J. R. Kan, "Injection of an electron beam into a plasma and spacecraft charging", *Phys. Fluids*, vol. 30, No. 1, p. 209, 1987.

[9] R. M. Winglee, and P. L. Pritchett, "Space charge effects during the injection of dense electron beams into space plasmas", *J. Geophys. Res.*, vol. 92, no. A6, p. 6114, 1987.

[10] H. Okuda, and J. Berchem, "Injection and propagation of a nonrelativistic electron beam and spacecraft charging", *J. Geophys. Res.*, vol. 93, no. A1, p. 175, 1988.

[11] R. M. Winglee, and P. L. Pritchett, "Comparative study of cross-field and field-aligned electron beams in active experiments", *J. Geophys. Res.*, vol. 93, no. A6, p5823, 1988.

[12] C. S. Lin and J. K. Koga, "Spacecraft charging potential during electron-beam injections into space plasmas", *IEEE Trans. Plasma Sci.*, vol. 17, no. 2, p. 205, 1989.

[13] R. Gendrin, "Initial expansion phase of artificially injected electron beam", *Planet. Space Sci.*, vol. 22, p. 633, 1974.

[14] C. W. Nielson, H. R. Lewis, "Particle simulation techniques in the nonradiative limit", *Methods Comput. Phys.* vol. 16, p. 367, 1976.

[15] R. W. Hockney and J. W. Eastwood, "Computer simulation using particles", McGraw-Hill, New York, 1981.

[16] D. E. Parks, A. R. Wilson, and I. Katz, "Monode plasma sheath dynamics", *IEEE trans. Nucl. Sci.*, vol. NS-22, no. 6, p. 2368, 1975.

FIGURE CAPTIONS

Fig. 1. Simulation configuration.

Fig. 2. Results of simulation for $n_b/n_c = 10$ and $v_b/a_c = 10$ at $\omega_{pe}t = 30$. (a) The beam electron phase space in the x-v_x plane and (b) the positions of beam electrons in the x-y plane. The position is normalized by the Debye length and the velocity is normalized by the initial beam injection velocity.

Fig. 3. Density plots of beam electrons at $\omega_{pe}t = 30$ for $n_b/n_c = 10$ and $v_b/a_c = 10$. (a) Contour lines delineate beam envelope. (b) Profile of beam density along beam showing maximum density close to spacecraft surface.

Fig. 4. Profiles of maximum field quantities across beam at $\omega_{pe}t = 30$. (a) Maximum transverse electric field E_y and (b) maximum longitudinal electric field E_x.

Fig. 5. Density plots of beam electrons at $\omega_{pe}t = 30$ for $n_b/n_c = 10$ and $v_b/a_c = 10$. Contour lines delineate beam envelope. Ω_{ce}/ω_{pe} = (a) 0.25, (b) 0.5, and (c) 1.0

Fig. 6. Electron beam envelope radius r_b/ρ_e versus n_b/n_c at $\omega_{pe} = 30$ for $v_b/a_c = 10$.

Fig. 7. Average velocity v_x at the stagnation point normalized to ambient electron thermal velocity a_c versus n_b/n_c at $\omega_{pe} = 30$ for $v_b/a_c = 10$.

Fig. 8. Electron beam envelope radius r_b/ρ_e versus initial beam injection velocity v_b/a_c at $\omega_{pe} = 30$ for $n_b/n_c = 10$.

Fig. 9. Absolute value of average velcity v_x at the stagnation point normalized to ambient electron thermal velocity a_c versus initial injection velocity v_b/a_c at $\omega_{pe} = 30$ for $n_b/n_c = 10$.

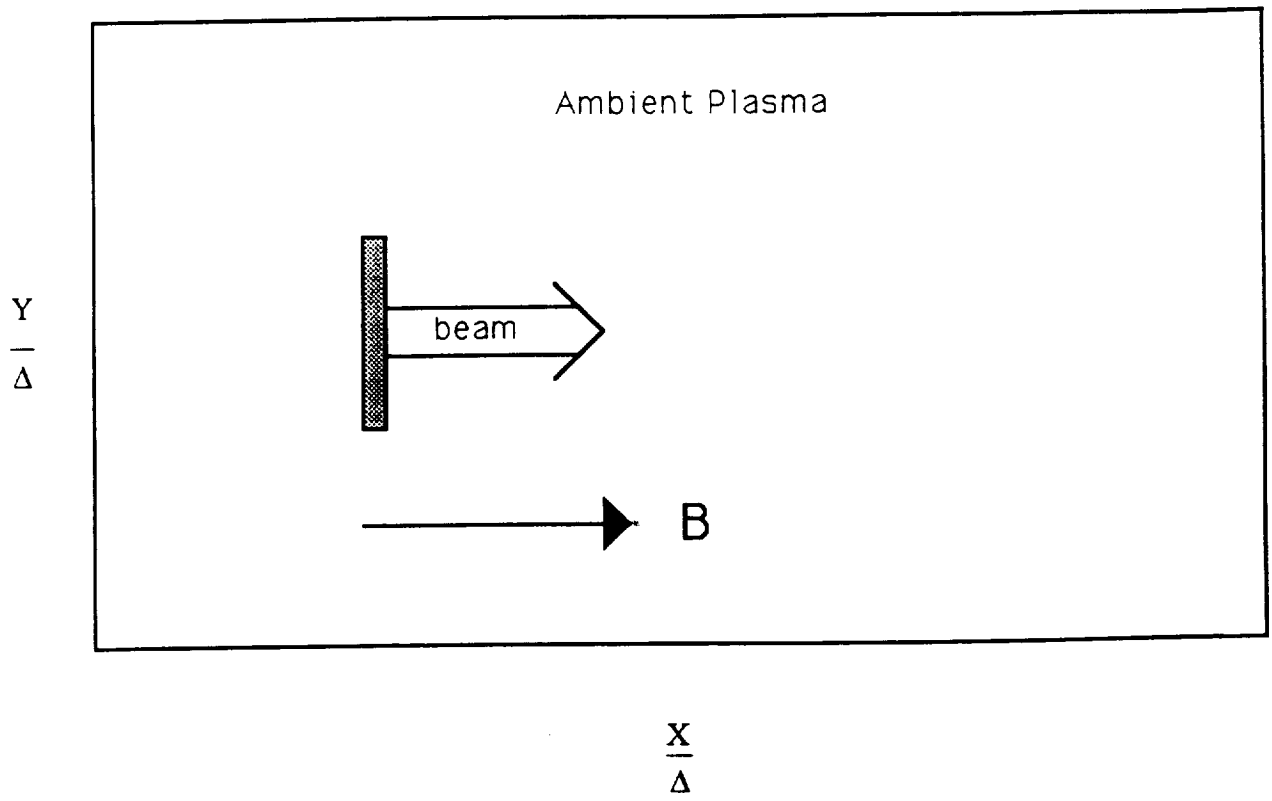

Figure 1

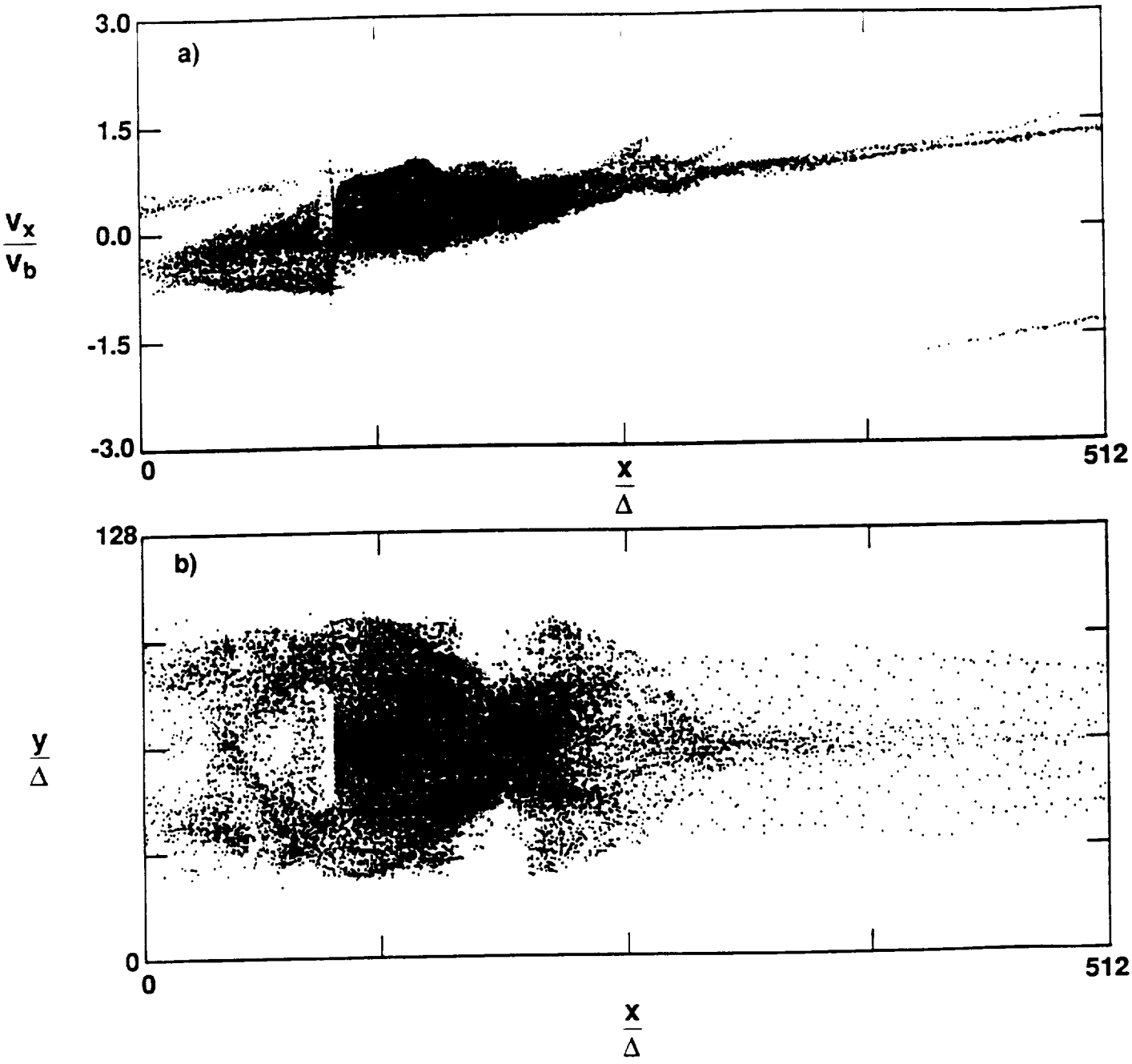
a)
3.0
1.5
0.0
-1.5
-3.0
$\frac{v_x}{v_b}$
0
512
$\frac{x}{\Delta}$
b)
128
0
0
512
$\frac{y}{\Delta}$
$\frac{x}{\Delta}$

Figure 2

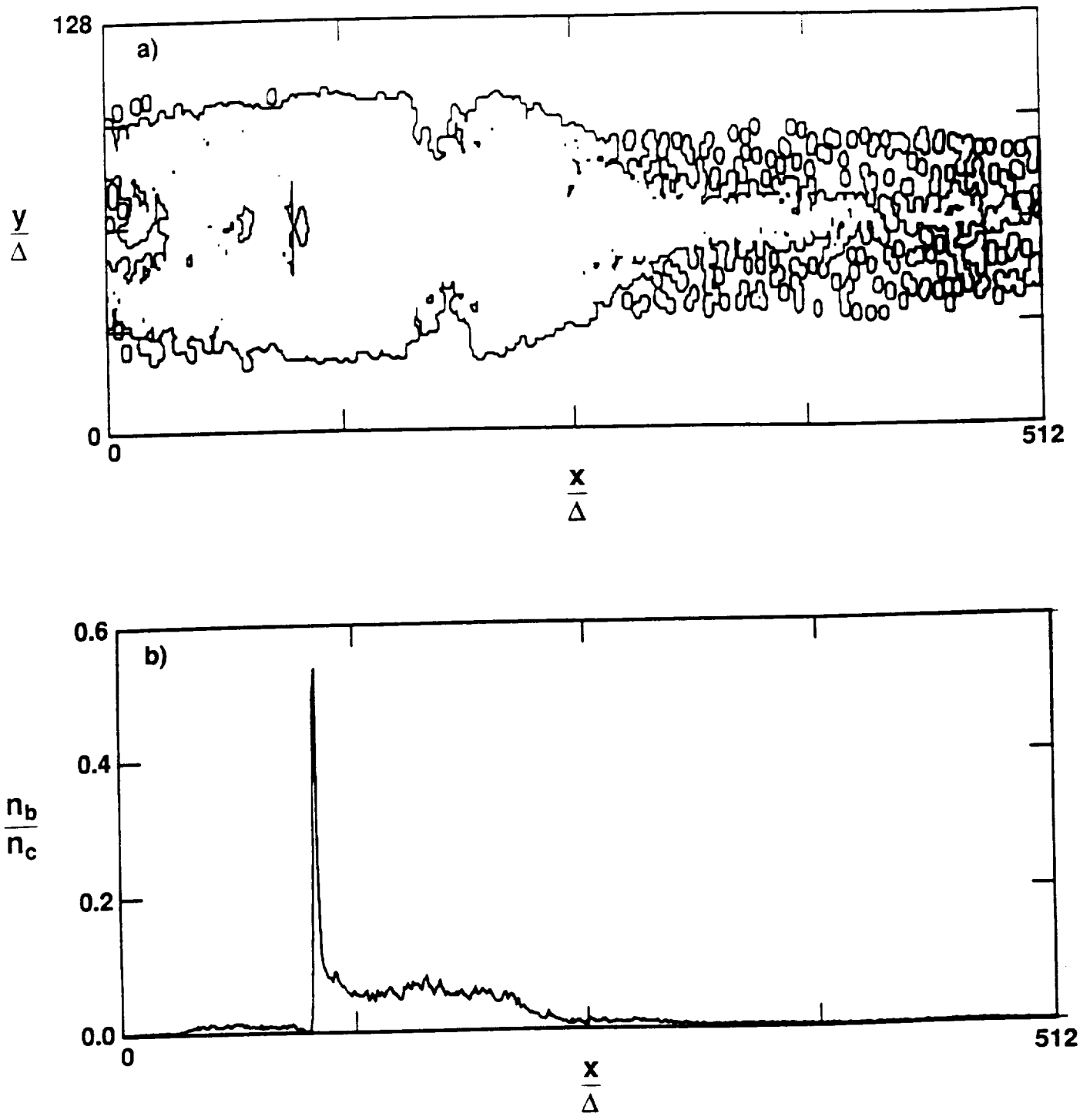

Figure 3

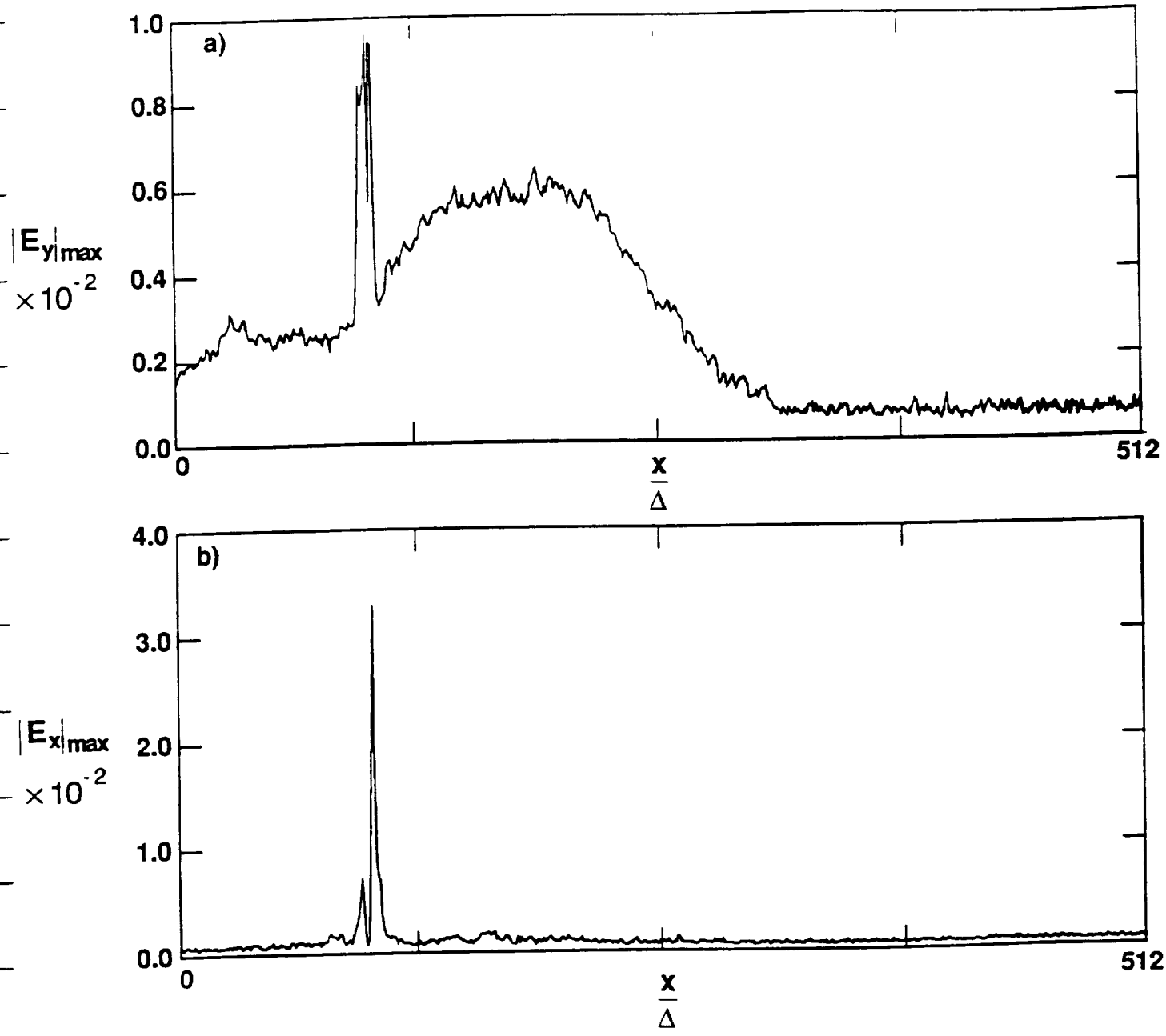
a)
1.0
0.8
0.6
0.4
0.2
0.0
$|E_y|_{max}$
$\times 10^{-2}$
0
512
$\frac{x}{\Delta}$
b)
4.0
3.0
2.0
1.0
0.0
$|E_x|_{max}$
$\times 10^{-2}$
0
512
$\frac{x}{\Delta}$

Figure 4

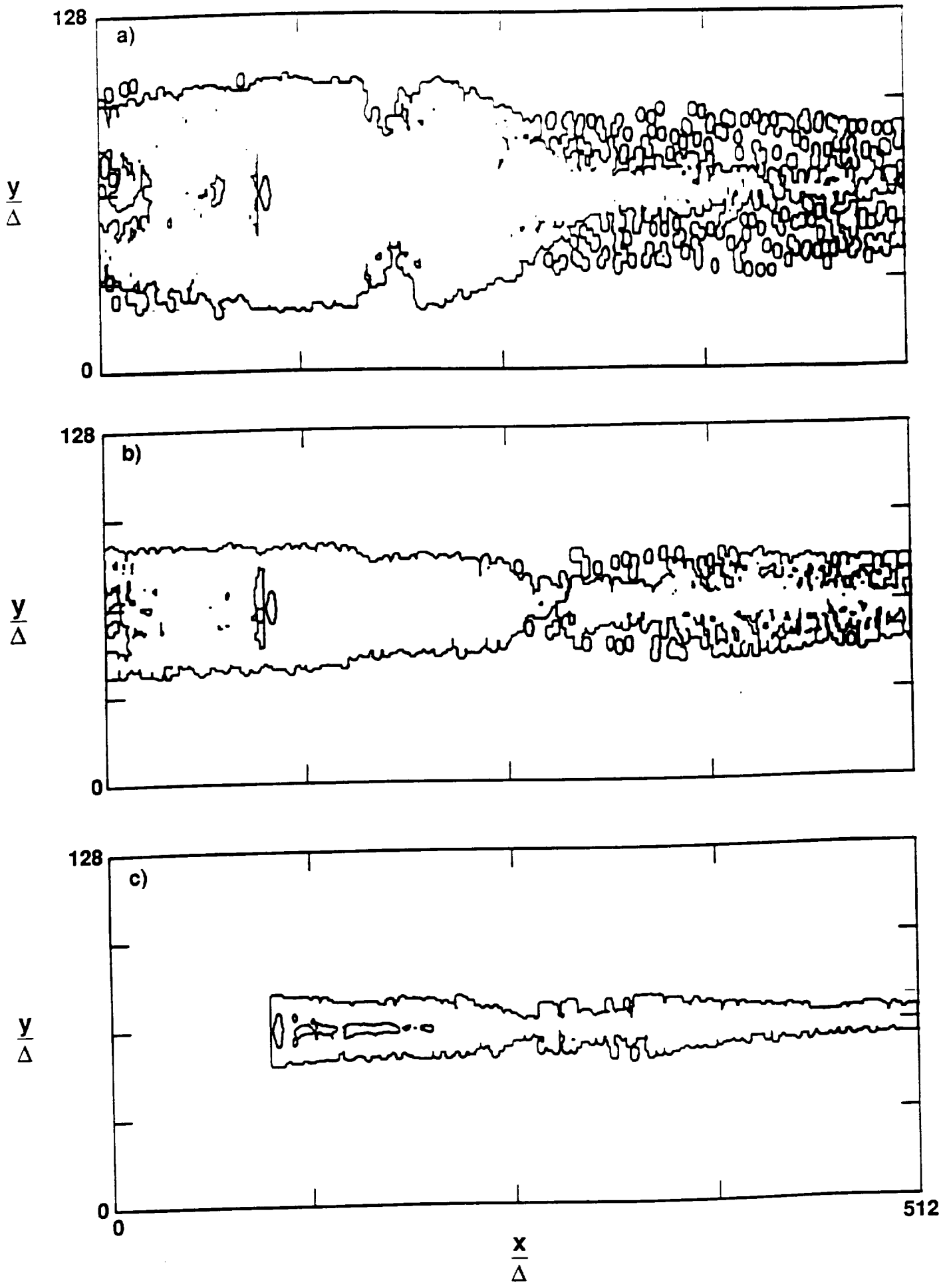

Figure 5

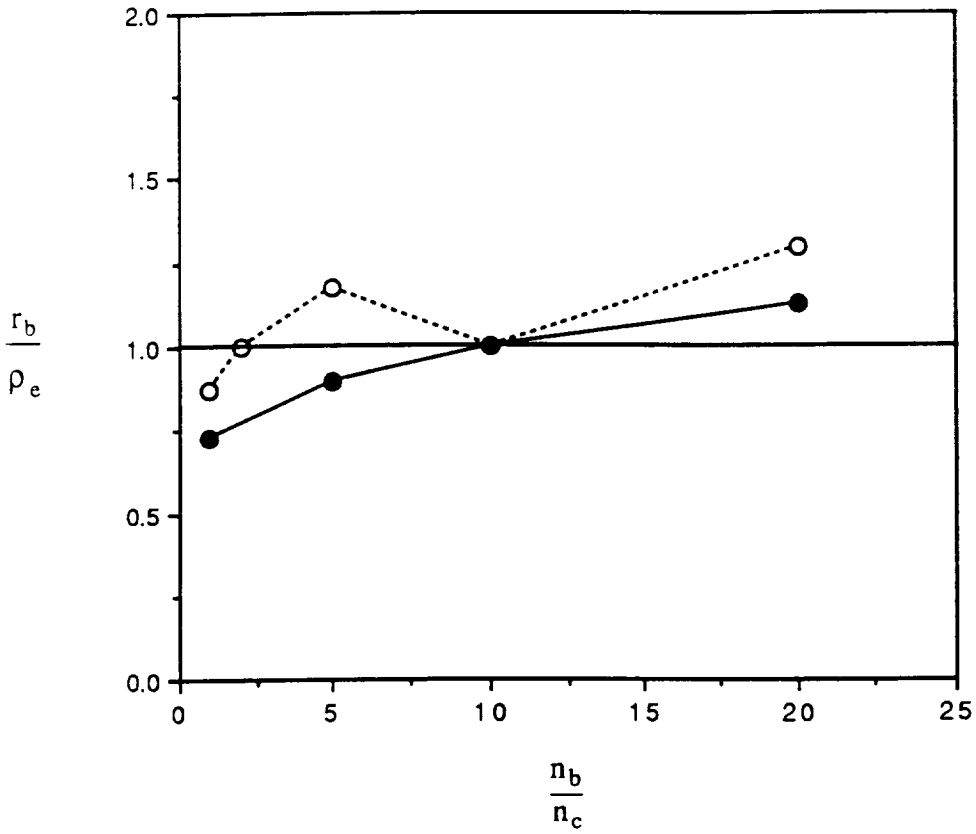

Figure 6

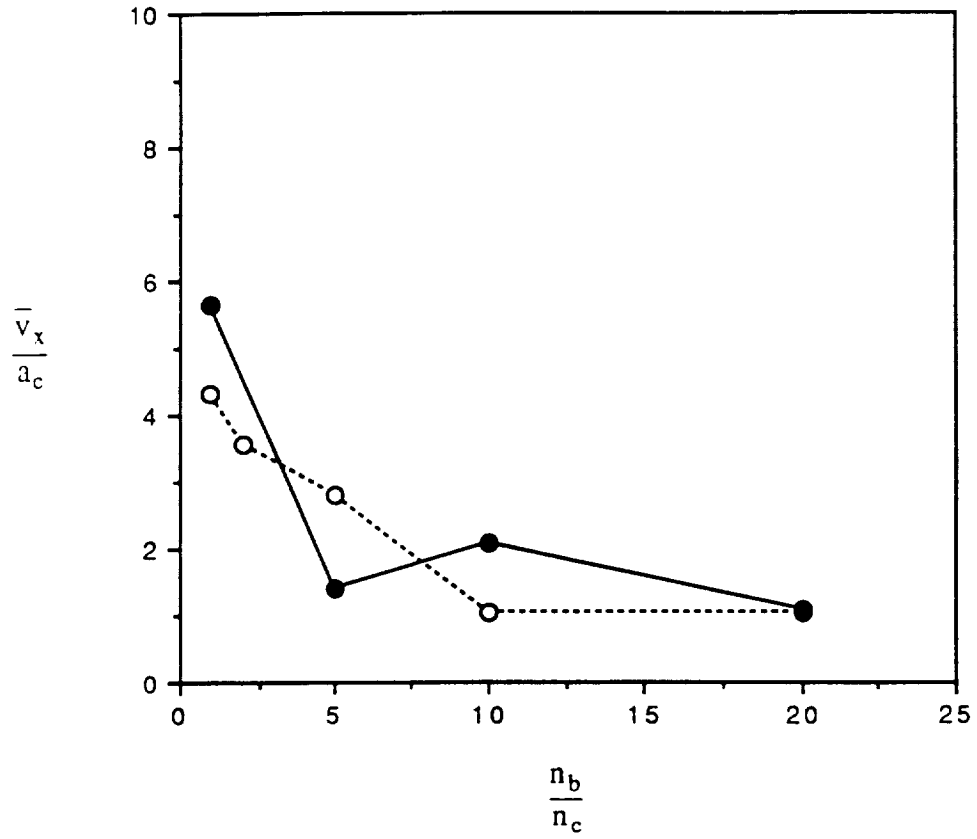

Figure 7

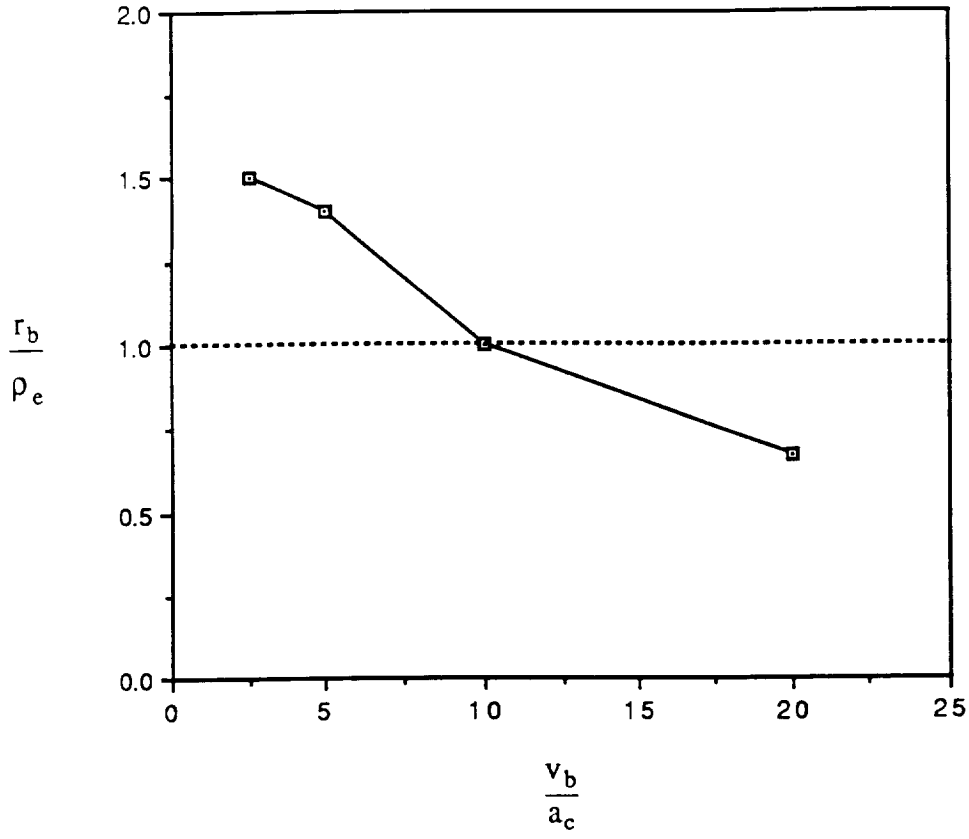

Figure 8

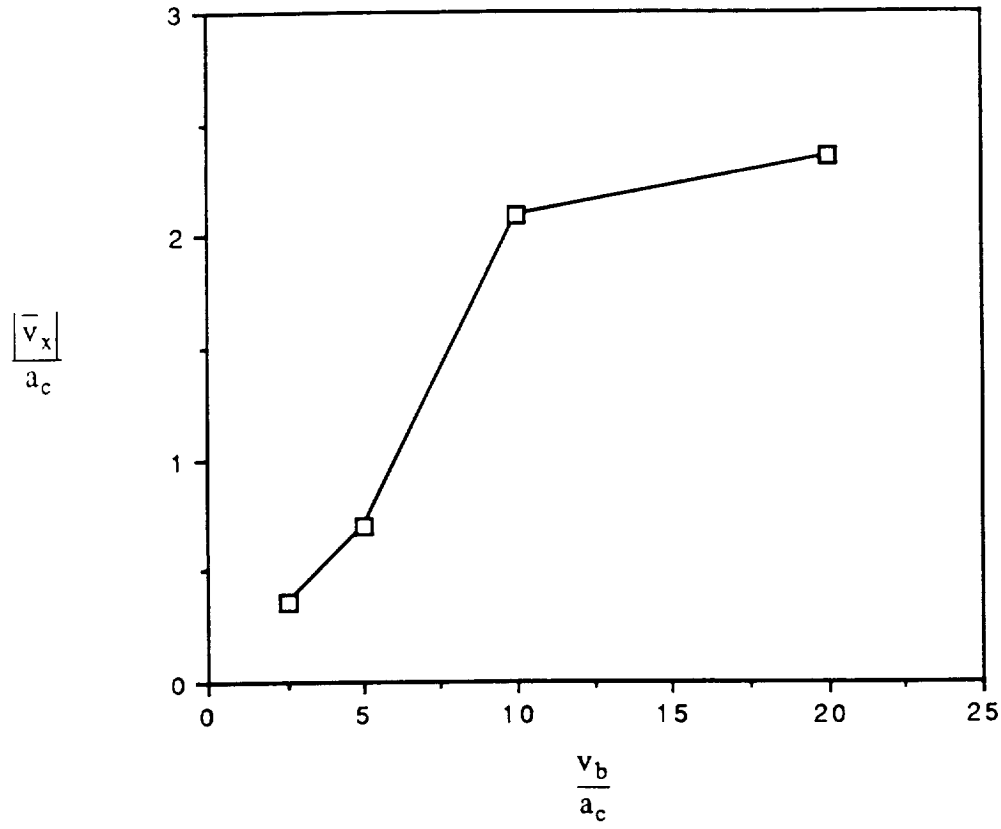

Figure 9